

C.E.R.N. CENTRE EUROPEEN DE LA RECHERCHE NUCLEAIRE

July 1, 1993

Direct measurement of the $b\bar{b}$ branching ratio at the Z^0 by hemisphere double tagging

- DELPHI Collaboration -

V. Castillo, J. Salt, E. Higón, E. Cortina, J. Marquina, F. Martinez

*IFIC, Centro Mixto Univ. of Valencia – CSIC,
Departamento de Física Atómica, Nuclear y Molecular,
Avda. Dr. Moliner 50, E-46100 Burjassot, Valencia, Spain.*

and

P. Billoir, H. Briand, C. de la Vaissière

*Laboratoire de Physique Nucleaire des Hautes Energies (L.P.N.H.E.)
Paris, France*

Abstract

This paper describes a direct evaluation of the $b\bar{b}$ hadronic branching ratio at the Z^0 peak ($x_b = \Gamma_{b\bar{b}}/\Gamma_{hadr}$) in DELPHI. This evaluation is basically independent of simulation models. The method uses the data from a Microvertex Detector and a tagging of b events based on a Multidimensional Analysis technique. Two independent fits are described which allow the extraction of x_b . The method applied on about 160000 events gives $x_b = 0.220 \pm 0.004 \pm 0.006$

1 Introduction

The aim of this paper is to present a new method to measure the fraction x_b of $b\bar{b}$ events produced at the Z^0 mass ($x_b = \Gamma_{b\bar{b}}/\Gamma_{hadr}$). This measurement, if determined enough accurately, has implications on the Standard Model parameters, in particular for the top quark mass [1]. A standard technique to perform this measurement is to use the prompt leptons produced in the quark b decay. However this allows to measure actually the product of x_b times the semileptonic branching ratio $b \rightarrow lX$. Up to now, most of the new techniques rely strongly on simulation models ; this is the main source of systematic errors.

We have already shown in a preliminary work [4], that it was possible to measure directly the composition of hadronic events by combining two independent taggings. The improved new method presented here is based on a Multidimensional Analysis tagging algorithm applied separately to the two hemispheres of an event ; this could be the first step towards the jet tagging for Higgs search at LEP 200 . At the Z^0 peak we can exploit the associated production of $q\bar{q}$ pairs of the same flavour. In order to discriminate beauty events from light quark events we shall use the relative long lifetime of the b hadrons (1.3 ps or even more according to recent evaluations) through a high precision tracking at the interaction point. The three layer micro-strip vertex detector of DELPHI allows to define observables sensitive to the decay in flight of b -hadrons.

Hemisphere tagging offers interesting possibilities if two conditions are fulfilled:

- 1) The tagging is the same in both hemispheres
 - 2) For a given flavour the taggings in the two hemispheres are uncorrelated.
- In this case, it is possible to extract the flavour composition of the sample directly from the data, together with the classification matrix necessary to compute the efficiencies and purities of the tags. As it will be explained, this is done without any explicit reference to the Monte Carlo simulation. By this way our determination is essentially free of bias. An other crucial advantage is that tagging one hemisphere does not bias physics in the opposite hemisphere. It can be combined also to other taggings - i.e. high p_t muon events -. In this article we concentrate on the simple determination of x_b . A separate paper [8] will describes how it is possible to measure the flavour composition and the hemisphere tagging matrix.

In section 2 we describe the selection and processing of the hadronic events. In section 3 we describe the principle of the extraction of x_b . Section 4 gives an overview of the tagging technique and of the level of its performances. Section 5 is devoted to the results, section 6 to a preliminary evaluation of systematic errors.

Event selection	Cut value
Number of charged particles (N_{ch})	$N_{ch} \geq 6$
Reconstructed mass (M)	$M \geq 16.GeV$
Reconstructed energy (E)	$E \geq 20.GeV$
Z of reconstructed vertex w.r.t. beam (Z_V)	$Z_V \leq 3.cm$
R of reconstructed vertex " " (R_V)	$R_V \leq 0.3cm$
$ \cos(\theta_s) $, where θ_s is the sphericity axis angle	$ \cos(\theta_s) \leq 0.75$
Number of charged particles required by hemisphere	$N_{ch}/hem \geq 6$

Table 1: Summary of cuts for event selection.

Track Selection	Cut value
momentum of charged particles (p)	$0.1 \leq p \leq 30. GeV$
momentum of neutral particles (p)	$2. \leq p \leq 30. GeV$
Distance to the main vertex in xy plane (d_{xy})	$d_{xy} \leq 1.0cm$
Track length (L)	$L \geq 40.cm$
$ \cos(\theta) $ where θ is the angle of the track:	
Charged	$ \cos(\theta) \leq 0.85$
Neutral	$ \cos(\theta) \leq 0.75$
R of starting track point (R)	$R \leq 45.cm$
$\Delta P/P$ for charged and neutrals	$\Delta P/P \leq 0.5$
ΔP for charged and neutrals	$\Delta P \leq 10.GeV/c$

Table 2: Summary of cuts for track selection.

2 Selection and processing of the hadronic events.

2.1 Description of the DELPHI Detector.

The DELPHI detector has been described in detail elsewhere [5]. Therefore we shall mention here only the features of the DELPHI vertex detector which is essential to our analysis:

The vertex detector in the 1991/92 configuration is formed by 3 concentric shells of Si-strips detector at radii of 6.5, 9 and 11 cm. It covers the central region over a length of 24 cm and defines an angular acceptance of $27^\circ - 153^\circ$, $37^\circ - 143^\circ$ and $42^\circ - 138^\circ$ for hits in one, two or three layers. Each layer is composed of 24 azimuthal modules with about 10% overlap in ϕ and each module is composed of 2x4 'plaquettes' along z . The intrinsic $r\phi$ resolution per layer to the beam axis has been evaluated to be $8\mu m$.

2.2 Track and event selection

The trajectories of charged particles include the microvertex hits after correction from the current alignment data base. The refitted trajectory is extrapolated to the 'perigee'¹, taking into account the crossed material in the error matrix. The neutral particles are

¹Point of closest approach of the helix to the z axis

included only for the calculation of sphericity and jet axes.

After this refit, the events are selected according table 1. The cosine sphericity cut at 0.75 ensures that most of the tracks are within the microvertex acceptance.

Table 2 gives the selection criteria of the particles to be used in the tagging.

3 Principle of the Method

Hadronic events at the Z^0 pole are produced in five flavour. In this analysis $u\bar{u}$, $d\bar{d}$, $s\bar{s}$ flavor were merged in a single uds family, since information on strange hadrons was not available and our tagging variables have the same distributions for the three flavours. This leaves us with 3 genuine families of events: uds , c and b .

Let us assume that a tagging algorithm provides an hemisphere tag depending on a purification cut δ and it is possible to increase the b-purity to almost 100% with non negligible efficiencies ². Let us call $C^{uds}(\delta)$, $C^c(\delta)$, $C^b(\delta)$ the probabilities that a uds , c or b hemisphere is tagged as b for a given value of δ .

The fraction of single tags $V_b(\delta)$ (for one hemisphere) may be expressed as:

$$V_b = C^{uds} x_{uds} + C^c x_c + C^b x_b$$

and the fraction $D_{bb}(\delta)$ of double tags (i.e. tagged equally in both hemispheres) is:

$$D_{bb} = (C^{uds})^2 x_{uds} + (C^c)^2 x_c + (C^b)^2 x_b$$

where x_{uds} , x_c and x_b are the flavour fractions in the sample.

In order to express these quantities in a more convenient way, we introduce the c and uds rejection powers as:

$$R_c(\delta) = \frac{C^c(\delta)}{C^b(\delta)}$$

$$R_{uds}(\delta) = \frac{C^{uds}(\delta)}{C^b(\delta)}$$

and the ratios of x 's :

$$\lambda_c = \frac{x_c}{x_b}$$

$$\lambda_{uds} = \frac{x_{uds}}{x_b}$$

Then :

$$V_b = C^b x_b (1 + \lambda_c R_c + \lambda_{uds} R_{uds})$$

$$D_{bb} = (C^b)^2 x_b (1 + \lambda_c (R_c)^2 + \lambda_{uds} (R_{uds})^2)$$

If the rejection powers $R_c(\delta)$ and $R_{uds}(\delta)$ tend towards 0 in the limit of high δ , and if we are able to evaluate C^b as a function of δ from the data themselves (through a selection

²The signification of the purification cut δ will be given in the tagging section.

of hemispheres such that the opposite hemisphere is highly purified in b through a strong cut on δ), we see that the ratios $\frac{V_b(\delta)}{C^b(\delta)}$ and $\frac{D_{bb}(\delta)}{(C^b(\delta))^2}$ tend towards x_b at high δ . We call this method the "indirect procedure".

We can also compute directly (independently of C^b) an interesting ratio giving asymptotically x_b :

$$r_1 = V_b^2/D_{bb} = x_b \frac{(1 + \lambda_c R_c + \lambda_{uds} R_{uds})^2}{1 + \lambda_c (R_c)^2 + \lambda_{uds} (R_{uds})^2}$$

This will be called the "direct procedure".

Experimentally we measure, for different values of the cut (δ_i), the following quantities: $N_b^1(\delta_i)$ and $N_b^2(\delta_i)$ which are the number of events with a single b tag in hemisphere 1 or hemisphere 2 respectively. $N_{bb}(\delta_i)$ which is the number of events with a double b tag. Then an estimator of $V_b(\delta_i)$ is given by $\frac{N_b^1(\delta_i)}{N_{tot}}$ or equivalently $\frac{N_b^2(\delta_i)}{N_{tot}}$; in the same way $D_{bb}(\delta_i)$ is estimated by $\frac{N_{bb}(\delta_i)}{N_{tot}}$, where N_{tot} is the total number of events in the sample. Then a measurement of r_1 , for example, is given by :

$$\frac{N_b^1(\delta_i) N_b^2(\delta_i)}{N_{bb}(\delta_i) N_{tot}}$$

The determination of asymptotic values through both procedures is given in Sect. 5.

4 Hemisphere tagging

The tagging algorithm should be viewed as a technique that classify the events or hemispheres into tags, which are enriched samples of chosen types. More important that the technique itself, would be here its efficiency. Multidimensionnal analysis has been chosen, as it provides a more efficient separation than a set of cumulated cuts. The details on the technique can be found in ref [7].

4.1 Partition into independent hemispheres

The aim is to subdivide the event into two sub-events, independent in all respects except the fact that they have the same flavour. The tagging of one hemisphere should be completely decorrelated from the tagging in the other hemisphere.

First the particles are partitioned in jets using the LUND algorithm LUCLUS with default parameters. Then the jet direction is defined from the internal thrust axis of the particles belonging to the jet. We use the main sphericity axis and the plane perpendicular to it to define the two hemispheres. The jets making an angle of less than 90^0 with this axis are attributed to hemisphere one, the others to hemisphere 2. All the particles of a jet are assigned to the hemisphere which the jet axis belongs to.

4.2 Reconstruction of hemisphere vertex

The position of the hemisphere vertex A_h is calculated through a robustification algorithm. First all the "central" charged particles in the hemisphere are included in a single vertex fit. If the fit probability is less than 0.05 the particle which contributes the most to χ^2 is removed, and a new vertex fit is attempted. The process continue until a probability over 0.05 is obtained or only two particles are left.

The beam spot center has been measured fill by fill, and this position has been used as a constraint in the fit with a r.m.s of $250\mu\text{m}$ in x and $50\mu\text{m}$ in y . In 1992 data, the size of the beam ellipse is $100\mu\text{m}$ in x and less than $40\mu\text{m}$ in y . Adding this constraint increases the discriminating power of the tagging. This beam spot constraint which is the only common feature of both hemispheres, introduce in principle no or little correlations. If the interaction point is exactly known, the requirement that the two hemisphere vertices coincide with their true position would improve decay length accuracies. It should not produce correlations. With a tight beam spot ellipse, the overwhelming majority of events are close to that situation. It is only when the true interaction point is far away from the ellipse, and the constraint forces it towards its center that a significant correlation can be introduced. A detailed study of eventual correlations can be found in ref.[8]...

4.3 Description of the tagging variables

The Multidimensional analysis is based on a set of 2×12 discriminant variables. This set is divided in two subsets, one for the hemisphere 1 and the other for the hemisphere 2, both with the same list of variables but computed in different hemispheres. The charged particles entering in the calculation of these variables are subject to tight cuts imposing that they are well reconstructed and have their origin close to the interaction point.

One variable per hemisphere (boosted sphericity) is computed only with quadrimomenta. The remaining variables use the parameters of the reconstructed trajectories at the perigee after quality cuts removing poorly reconstructed tracks. Four of them are connected to the χ^2 fit of vertices associated to various sets of particles. Three are distances between a "candidate secondary" vertex and the primary vertex and are sensitive to decay ranges of c and b-hadrons. The last four variables are estimators of the number of secondary particles and of the total energy and p_t^2 associated to them.

A full description of these cuts and of the variable definition can be found in ref [7].

4.4 Tagging algorithm

4.5 Obtention of tags

Each set of 12 variables is used to compute three probabilities p_{uds} , p_c and p_b for an hemisphere to have the uds, c and b flavour. This calculation is based on a Monte-Carlo modelisation. The flavor probabilities are sorted in decreasing order as p_{first} , p_{second} , etc. The hemisphere is tagged uds, c or b accordingly to the highest probability p_{first} .

At this stage, a "winner margin" $\Delta = \ln(p_{first}/p_{second})$ appears a sensitive indicator of ambiguity. We can improve the b tag purity by the condition $\Delta > \delta$ where δ is the value of the cut mentionned in section 3.

4.6 Results obtained on simulation

The quality of the tagging can be inferred from results obtained on a full simulation that includes the effect of the apparatus. We shall describe mainly only the features of the single and double hemisphere b-tags. The results were obtained on 168861 simulated events.

- Figs. 1.a and 1.c show the purity and the efficiency of the simple hemisphere b-tag as a function of the purification cut δ . It can be seen that the purity succeeds in

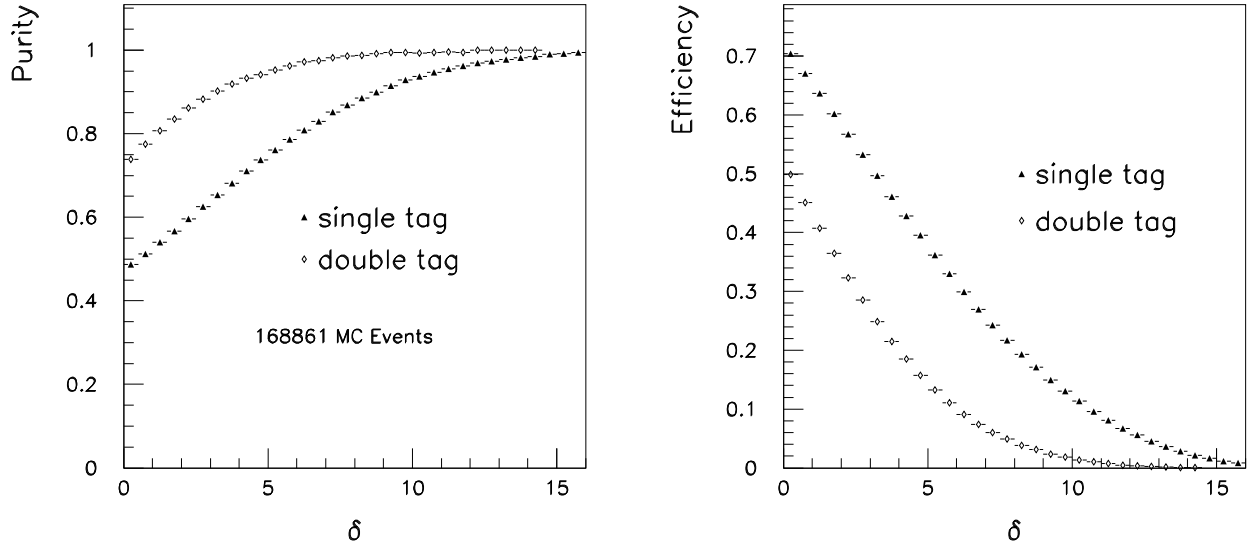


Figure 1: *Performances of single and double hemisphere b-tagging estimated on simulated events: a) Purities, b) Efficiencies of single and double b-tags*

approaching the level of 100%, but at the cost of a low efficiency. The purity and the efficiency of the double hemisphere b-tag are plotted on Figs. 1.b and 1.d. Without any δ cut the double b-tag purity is already 75%, and approaches rapidly 100% with a δ cut, with still appreciable efficiencies. Above $\delta > 6.0$ double-tagged b events can be considered practically pure.

- Fig. 2 shows the variation with δ of the fractions of single and double b-tags V_b and D_{bb} . The comparison between real data and simulation indicates a similar behaviour but a shift is observed in absolute values. The (absence of) influence of this shift on the determination of x_b will be discussed later.
- Fig. 3-a shows the composition on simulation of the b tag as a function of the clear winner margin Δ . In Fig. 3-b the rejection powers $R_c(\delta)$ and $R_{uds}(\delta)$ are plotted. As expected the drop of R_{uds} is much faster. Both can be parametrized by a second order exponential dependence in δ .

5 Results on the measurement of x_b

5.1 Direct procedure

On Fig 4.a, the ratio $r_1 = \frac{N_b^1(\delta_i)N_b^2(\delta_i)}{N_{bb}(\delta_i)N_{tot}}$ is plotted versus the purification cut δ , from 160861 real hadronic events taken in 1991 and passing the selection. The asymptotical behaviour of the curve is visible.

It should be pointed out that in the expression of r_1 the contents of the different bins are correlated: The $N_b^1(\delta_i)$ events selected with the cut δ_i are a subset of the ones selected with $\delta_j < \delta_i$. Similarly $N_b^1(\delta_i)$ and $N_{bb}(\delta_i)$ are imbedded in $N_b^2(\delta_j)$ and $N_{bb}(\delta_j)$ respectively.

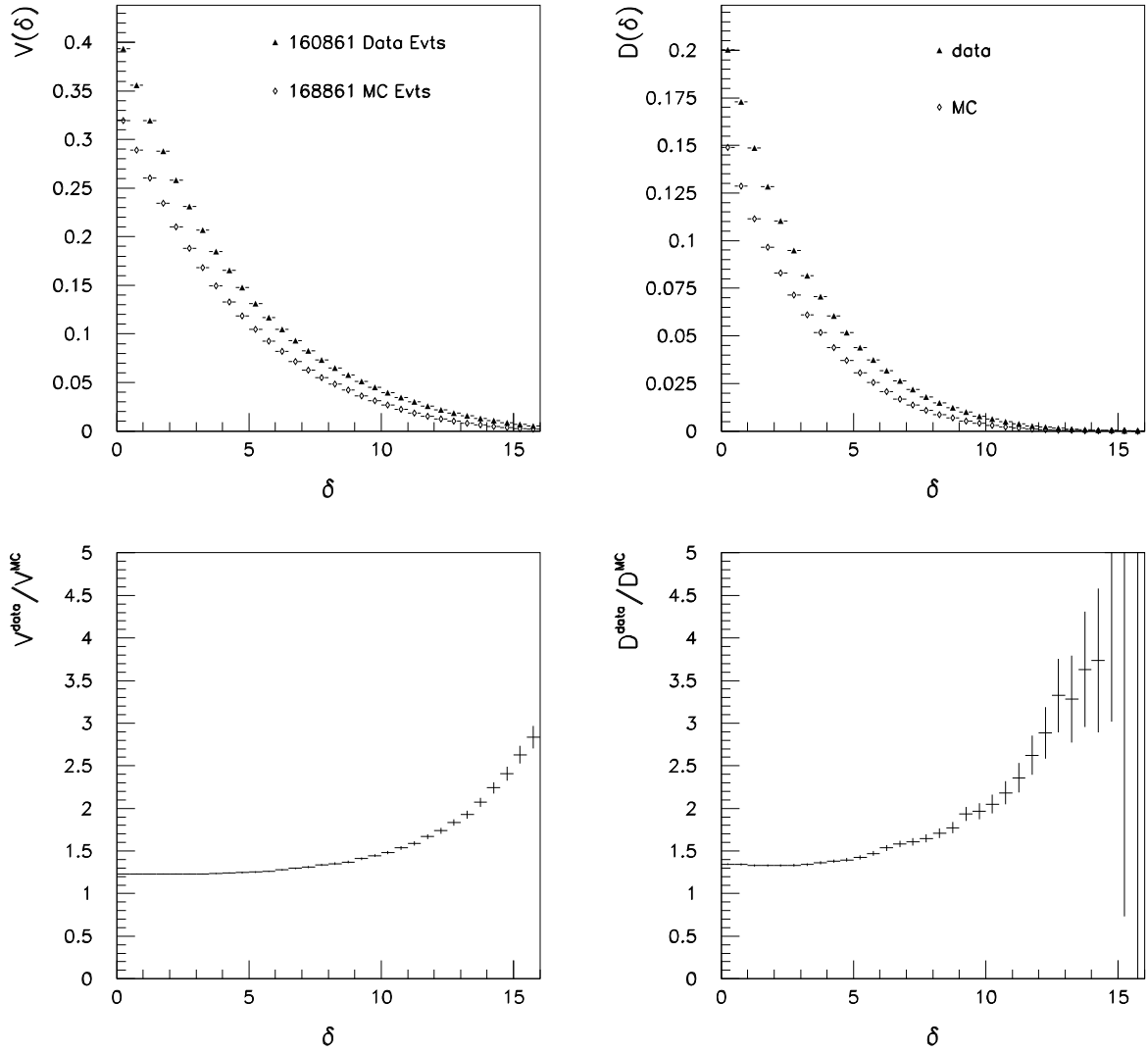


Figure 2: *Distributions of the fractions of single and double b-tags with respect to δ . a) Fractions of single b-tags $V_b(\delta)$ for real data and Monte-Carlo; b) Distributions of the double b-tag fraction $D_{bb}(\delta)$; c and d) Ratios of these fractions between data and Monte-Carlo (1.2 ps)*

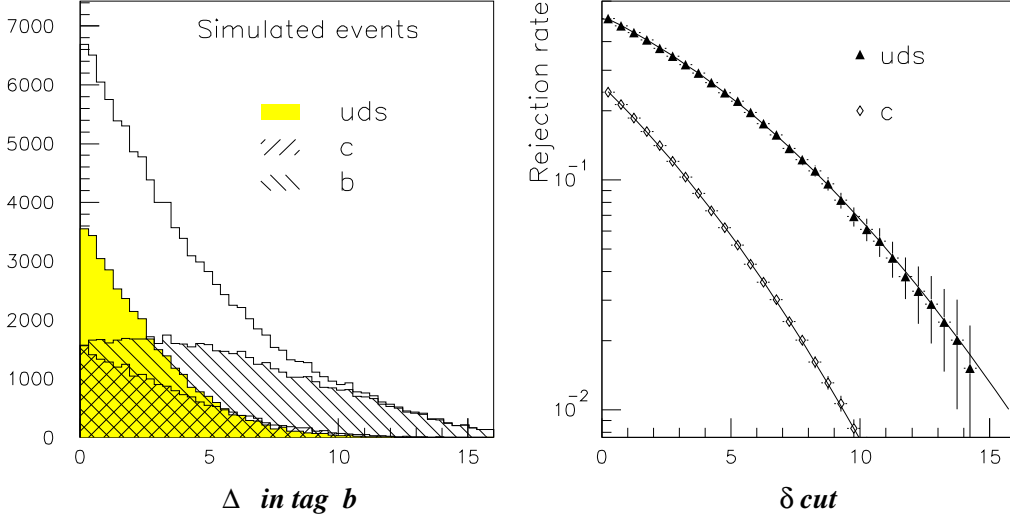


Figure 3: a) Distribution of the clear winner margin Δ in the b tag obtained on 168661 simulated events and contributions of the 3 flavours. b) uds and c rejection rates R_{uds} and R_c as a function of the clear winner cut δ .

For this reason, two different approaches have been used to extract x_b from the data and to evaluate properly the statistical errors :

- 1) We computed the full bin-to-bin covariance matrix $cov(r_1(\delta_i), r_1(\delta_j))$ and we used its inverse to compute the χ^2 to be minimized in the fit.
- 2) We removed most of this interbin correlation by defining the "decorrelated" ratio (see Fig 4.b):

$$r_2 = \frac{N_b^1(\delta_i)N_b^2(\delta_i) - N_b^1(\delta_{i+1})N_b^2(\delta_{i+1})}{(N_{bb}(\delta_i) - N_{bb}(\delta_{i+1}))N_{tot}}$$

The property of r_2 is to reach the same limit of r_1 in the region of large values of δ . In this expression the correlation vanishes in the denominator, which gives the dominant contribution to the statistical error.

The following step is then to choose a parametrization to find the asymptote.

We have tried, first, an empirical and simple parametrization of $r_1(\delta)$: It has been observed on simulation that $r_1(\delta)$ is adequately described by a simple expression ³:

$$r_1 = x_b + p_1 \exp(-p_2 \delta - p_3 \delta^2)$$

When fitting the data with 4 parameters (x_b , p_1 , p_2 and p_3) we find

$$x_b = 0.219 \pm 0.009$$

³In the full expression of r_1 the denominator tends rapidly towards 1 and is practically constant. The expression in the numerator, which is squared, is dominated by the variation of R_c and R_{uds} . It is a sum of second order exponentials tending towards zero. This may explain why the simple parametrization by a second order exponential plus a constant term is adequate.

compatible with the previous estimations. Moreover, this simple parametrization can be used also to represent the "decorrelated" ratio r_2 . The distribution of this ratio is given for data on Fig 4.b. A similar fit (without accounting for remaining interbin correlations) gives:

$$x_b = 0.217 \pm 0.010$$

The value and its statistical errors agree with the previous ones based on r_1 .

An alternative, is to use the theoretical expression of r_1 . As explained in section 3, the theoretical expression of r_1 is :

$$r_1(\delta) = \frac{(x_b + x_c R_c(\delta) + x_{uds} R_{uds}(\delta))^2}{x_b + x_c (R_c(\delta))^2 + x_{uds} (R_{uds}(\delta))^2}$$

where the rejection rates R_c and R_{uds} are functions of δ , which can be parametrized, according to Monte-Carlo data by (Fig.3.b).

$$R_{uds}(\delta) = p_1 \exp(-p_2 \delta - p_3 \delta^2)$$

$$R_c(\delta) = p_4 \exp(-p_5 \delta - p_6 \delta^2)$$

The fit with 8 parameters (x_b, x_c, p_1 to p_6) offers too many degrees of freedom to fit a monotonous, decreasing distribution. However, as will be described for the indirect procedure, it is possible to measure $C_b(\delta)$. This measurement can be used to compute the parameters $p_1 = R_{uds}(0)$ and $p_4 = R_c(0)$ for any given set of x_{uds}, x_c and x_b .

The b-tag efficiency $C_b(0)$ has been measured to be 0.763 with an error smaller than 0.01. $C_{uds}(0)$ and $C_c(0)$ are solutions of the two equations

$$V(0) - C_b(0)x_b = C_{uds}(0)x_{uds} + C_c(0)x_c$$

$$D(0) - C_b^2(0)x_b = C_{uds}^2(0)x_{uds} + C_c^2(0)x_c$$

From $C_{uds}(0)$ and $C_c(0)$, an estimator of p_1 and p_4 can be computed. This procedure forces the fitted curve to pass exactly through the first measured point, which is the most far away from the asymptote. It will not affect the value of the asymptote itself. By this technique, the number of parameters in the fit can be reduced to 6 and even 5, if x_c is fixed. We find :

$$x_b = 0.209 \pm 0.009$$

(the variation of x_c from 0.16 to 0.20 induces a negligible variation ± 0.0005 on x_b)

5.2 Indirect procedure

This procedure is intended to give a faster convergence, and thus to exhibit more clearly the asymptotical behaviour. We can estimate $C^b(\delta)$ in one hemisphere, when the condition of full b-purity is reached in the opposite hemisphere. We estimate $C^b(\delta)$ for a given value of δ as the limit , for high δ' , of the ratio $N_{bb}^{12}(\delta, \delta')/N_b^2(\delta')$, or equivalently $N_{bb}^{12}(\delta', \delta)/N_b^1(\delta')$, where $N_{bb}^{12}(\delta, \delta')$ is the number of events satisfying the cut δ in hemisphere 1 and δ' in hemisphere 2. Fig.5 shows the value of the ratio above for a given value of δ as a function of δ' : the asymptote is clearly visible ; In practice, we have chosen $\delta' = 12$ to compute

Fig 4 : Direct procedure

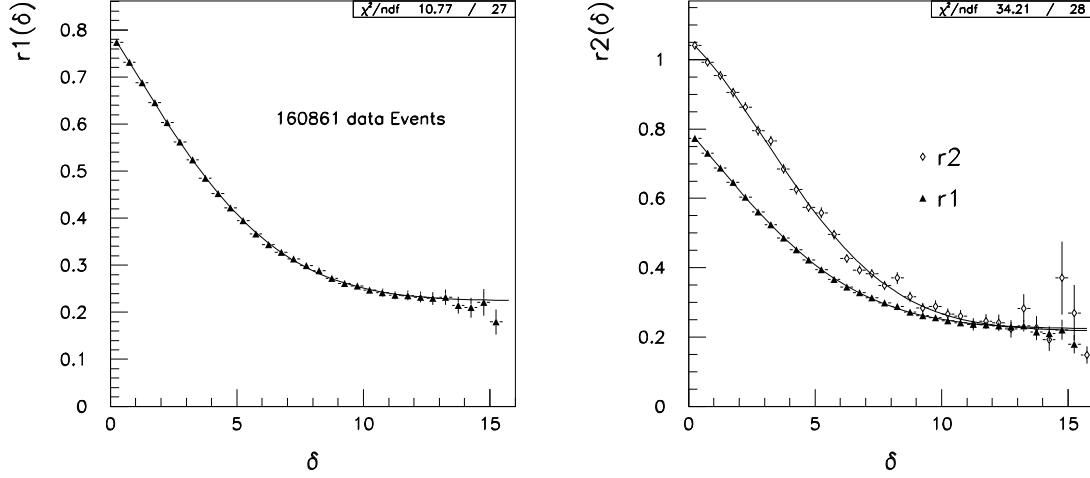


Figure 4: a) Distribution of the ratio $r_1(\delta)$ on 160861 real hadronic events. The curve correspond to the simple fit by a constant plus a second order exponential. b) Distribution of the "decorrelated" ratio $r_2(\delta)$, fitted by the same parametrization and compared to $r_1(\delta)$.

an estimation of C^b . 7108 hemispheres on real data and 4293 on simulation pass this condition of b-purity. Fig.6.a shows C^b as a function of δ . Again, the statistical errors on different bins are correlated, and we introduced as above the "decorrelated" quantities $\Delta C_i^b = C^b(\delta_i) - C^b(\delta_{i+1})$, shown on Fig.6.b .

In the second step, we build estimators of $V_b(\delta_i)/C^b(\delta)$ and $D_b(\delta_i)/C^b(\delta)^2$ introduced in Sect.3 :

$$s_1 = \frac{N_b^1(\delta_i)}{N_{tot}C^b(\delta_i)} \quad \text{and} \quad t_1 = \frac{N_{bb}(\delta_i)}{N_{tot}(C^b(\delta_i))^2}$$

In order to avoid inter-bin correlations, we shall use instead of s_1 and t_1 , "bin-to-bin decorrelated" ratios which are respectively :

$$s_2 = \frac{(N_b^1(\delta_i) - N_b^1(\delta_{i+1}))}{N_{tot}(C^b(\delta_i) - C^b(\delta_{i+1}))} \quad \text{and} \quad t_2 = \frac{(N_{bb}(\delta_i) - N_{bb}(\delta_{i+1}))}{N_{tot}((C^b(\delta_i))^2 - (C^b(\delta_{i+1}))^2)}$$

These ratios have the same asymptotical value x_b as s_1 and t_1 .

Fig.7.a shows the evolution of the new decorrelated ratios s_2, t_2 : as expected, the convergence is faster for t_1 and t_2 (in t_2 the rejection powers R_c and R_{uds} are squared), and the plateau is now obvious ; both curves appear to be compatible with the same asymptotical value. The statistical errors are obtained by combining the errors on uncorrelated numbers of events with the errors on the differential C_b previously computed. We fitted the dependence in δ with a constant plus an exponential (in order to avoid correlations between the numerator and the denominator, the fit is limited to the region $\delta < 12$).

Without smoothing the C_b and ΔC_b distributions, the results are, based on for s_2 ,

$$x_b = 0.221 \pm 0.013$$

and for the evaluation with t_2

$$x_b = 0.222 \pm 0.008$$

Fig 5 : Extraction of Cb

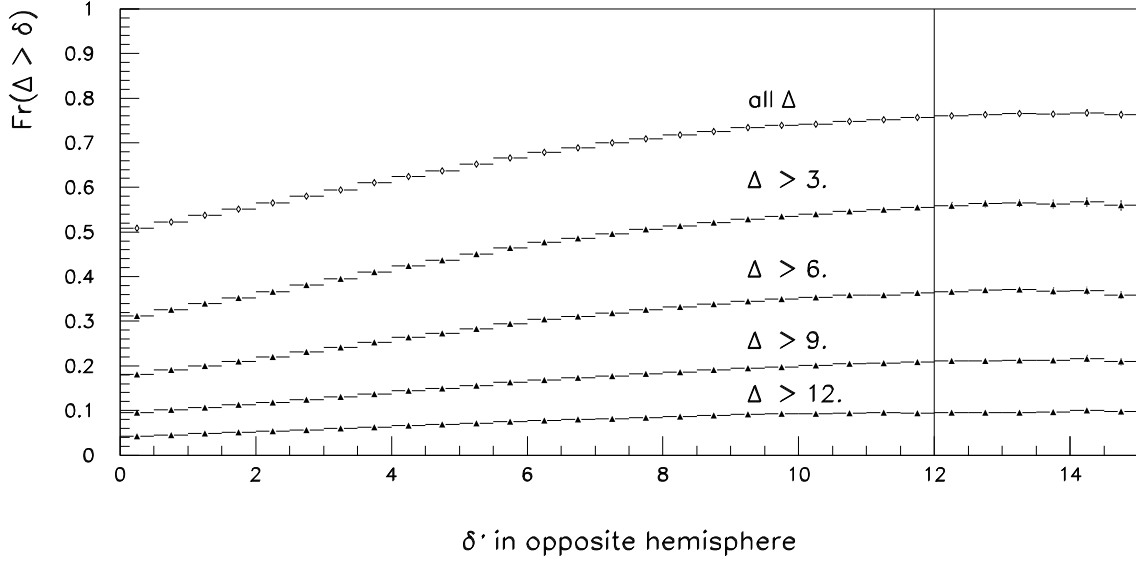


Figure 5: Principle of the determination of $C_b(\delta)$. The fraction of hemispheres tagged b with the additional condition $\Delta > \delta$, as a function of the purification cut δ' in the opposite hemisphere. The fractions are plotted for a set of values of δ .

Fig 6 : Distribution of C_b and ΔC_b

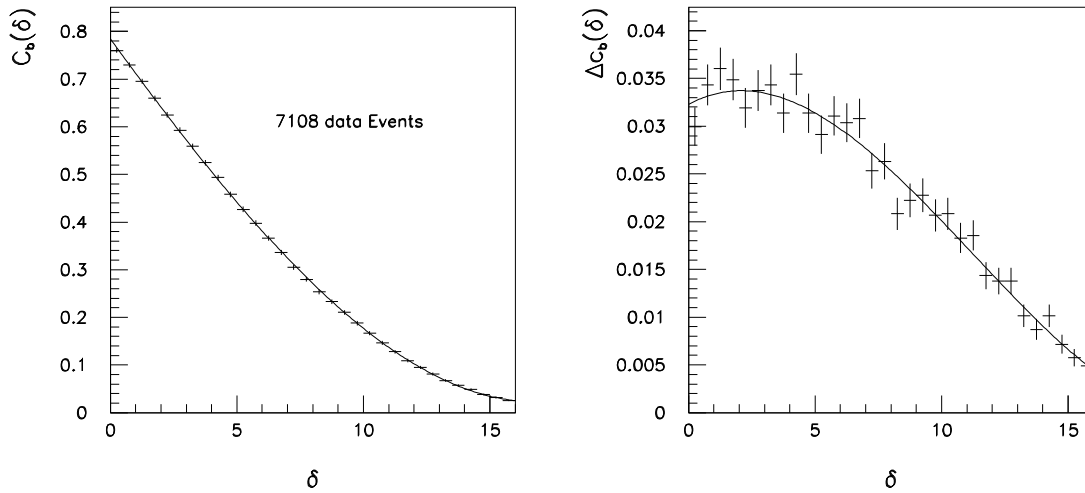


Figure 6: Classification probabilities of b events in the b -tag, estimated by the previous method as a function of δ : a) b -tag efficiency $C_b(\delta)$; b) Differential probability, $\Delta C_b(\delta)$. Both distributions are accurately described by a third order polynomial in δ .

Fig.6.a and b shows that a third order polynomial fit gives a satisfactory smoothing on the C_b and ΔC_b distributions in the whole range of δ , with a statistical uncertainty of the order of 0.0005, i.e. a few percent of its value in the range $0 < \delta < 12$. In order to reduce the errors in the denominators of s_2 and t_2 , we have replaced the C_b and ΔC_b by the values of the third polynomial fits of these quantities. After this smoothing, the results are with s_2 ,

$$x_b^{s_2,smooth} = 0.226 \pm 0.007$$

and with t_2

$$x_b^{t_2,smooth} = 0.216 \pm 0.005$$

5.3 Monte-Carlo cross-check

A cross-check has been performed on a Monte-Carlo hadronic sample of comparable size to the data (168861 evts after cuts). These events were generated with the same 1.2 ps lifetime for all b-hadrons ⁴. It was observed that the distribution in δ is less extended in simulation than in real data : this can be mainly due to the underestimation of the simulated lifetime (1.2 ps) ; as a consequence, the tagging is more efficient at high purities in real data, and the statistical errors on x_b are better.

In the analysed MC sample, the true fraction of b-events within the acceptance is $x_{b,true} = 0.222$, The results of a fit by a constant term plus a second order exponential is shown in Fig.8. The value of the asymptote is

$$x_{b,MC}^{fit} = 0.207 \pm 0.013$$

Fitting r_2 instead of r_1 gives

$$x_{b,MC}^{fit} = 0.209 \pm 0.013$$

in agreement with the previous value, but one σ lower than the expected value. By selecting only genuine b-events in the b-tag, we have plotted also the ratios r_1^{ideal} and r_2^{ideal} that would be observed in the absence of uds and c contaminations. These ratios should be independent of δ , if there is no correlation between hemispheres,. The distribution of r_1^{ideal} shows a small drop for large values of δ which could be the source of a systematic effect in the estimation of the asymptote. This drop is due to an small excess of double-tags events at the end of the spectrum, which is scarcely populated.

For the indirect method, Monte-Carlo allows in addition to check the validity of the $C_b(\delta)$ estimation, by comparing it to its true value $C_b^{true}(\delta)$, which is the b-tag efficiency for b-events. The Fig.9.a compares the estimated and true $C_b(\delta)$, and suggest an close agreement. The agreement can be better checked on Fig.9.b, where the relative differences between the two quantities is plotted. Up to a value of $\delta < 12$. the agreement remains within 1% in relative value.

The Fig.8.c and d plot the decorrelated ratios s_2 and t_2 , obtained after smoothing of the distributions of C_b and ΔC_b . The results

$$x_{b,MC}^{s_2,smooth} = 0.221 \pm 0.007$$

⁴This simulation should be distinguished from the one needed for the modelisation of the tagging: The two samples were produced with different versions of the simulation/analysis chain, so that efficiencies and errors on trajectories. They happen to differ significantly. In that way, we mimic in the simulation possible discrepancies between the model used for the tagging and real data. This is important to show that the x_b measurement is model independant

Fig 7 : Fits of s and t ratios

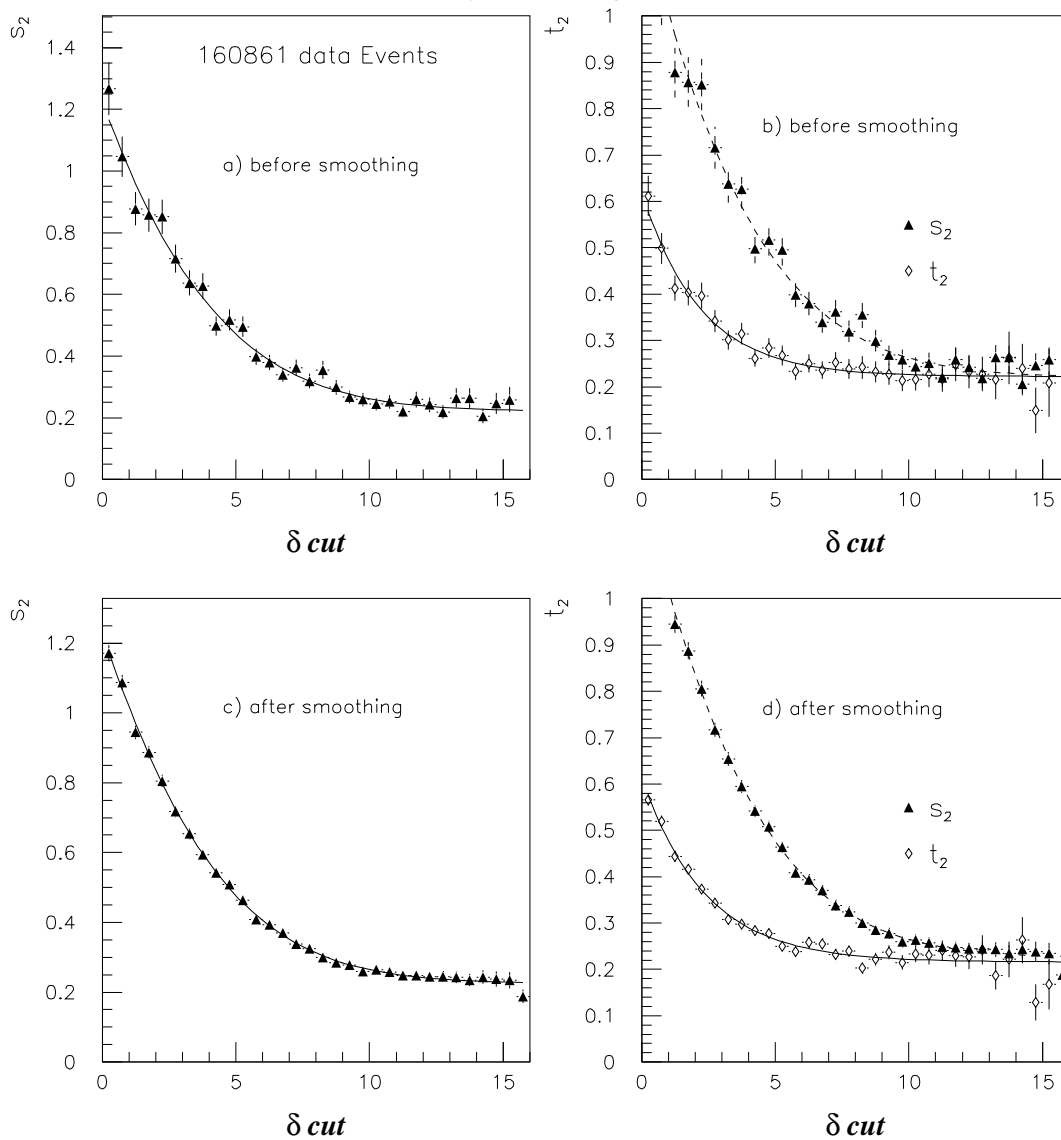


Figure 7: Ratios s_2 and t_2 on 160861 real events, and fit for the extraction of the asymptotical values : a) and b) Without $C_b(\delta)$ smoothing ; c) and d) with $C_b(\delta)$ smoothing.

Fig 8 : Fits of r, s and t ratios on MC

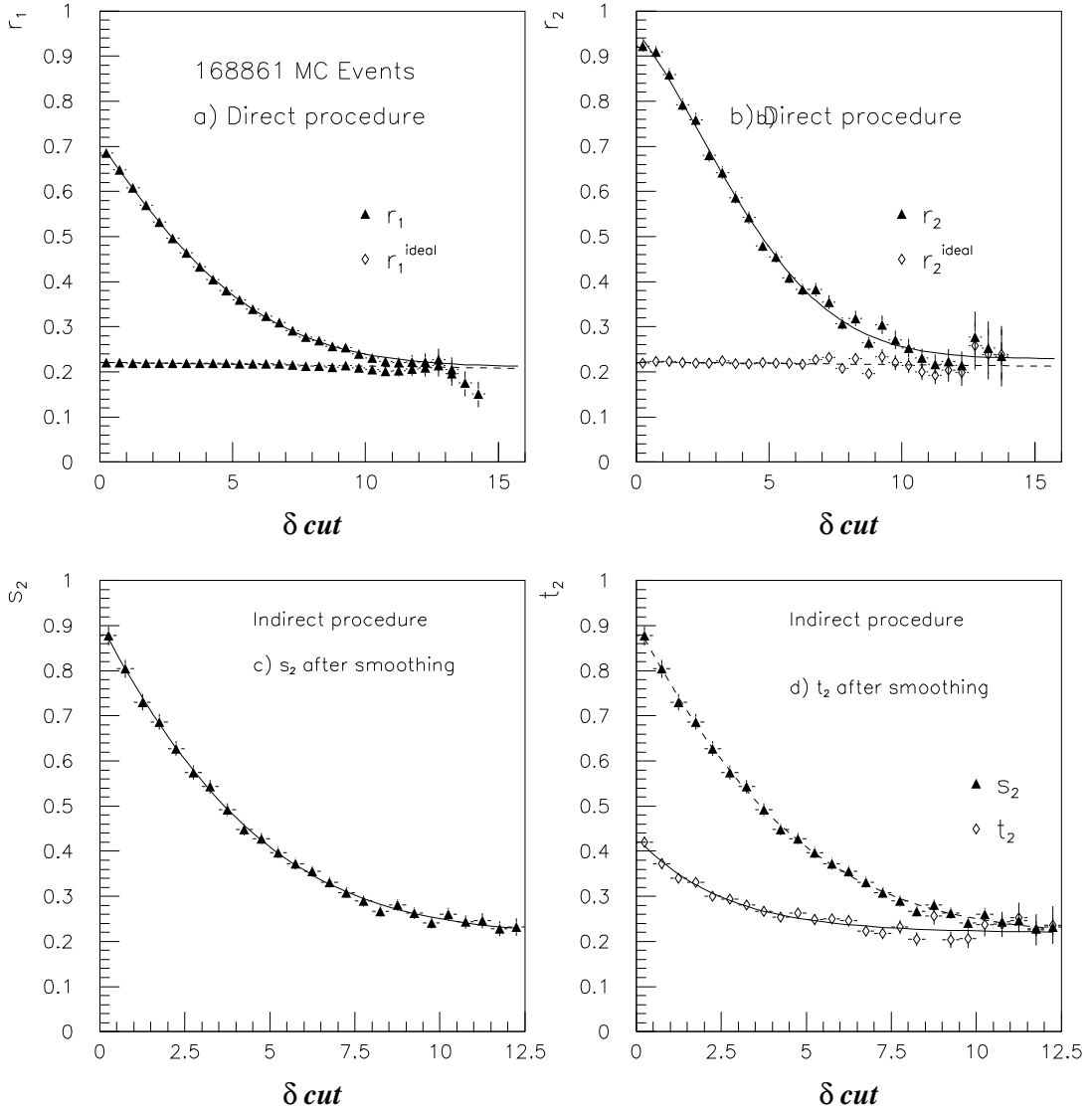


Figure 8: a) Fit of $r_1(\delta)$ on a simulated sample ; r_1^{ideal} (flat distribution) is the same ratio when the uds and c contaminations have been removed. b) Same as before but for the "decorrelated" ratio r_2 ; c and d) Indirect measurements : decorrelated ratio s_2 , t_2 after smoothing of $C_b(\delta)$

Fig 9 : Cross-check of C_b distributions

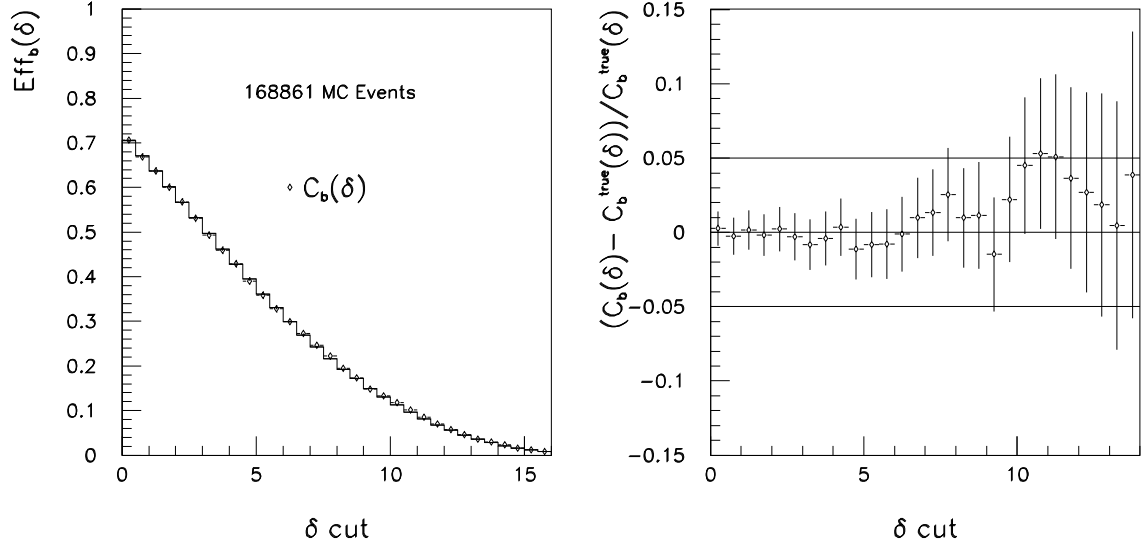


Figure 9: Check on the simulated sample of the asymptotical estimation of the $C_b(\delta)$ probabilities. a) Comparison of the estimated $C_b(\delta)$ with the true tag efficiency $C_b^{true}(\delta)$. b) Plot of the relative difference $(C_b(\delta) - C_b^{true}(\delta))/C_b^{true}(\delta)$.

$$x_{b,MC}^{t_2,smooth} = 0.219 \pm 0.007$$

respectively for s_2 and t_2 , are in better agreement with the 0.222 expected value than the results with the direct ratios r_1 and r_2 . The better agreement is due to the removal in the fits of the region $\delta > 12$, which is possibly affected by residual correlations.

6 Systematic errors

The study of systematic errors is still in a preliminary status. We have considered the following sources of errors, estimated from simulation:

- **Error due to the technique of estimation of the asymptote :**

A first evaluation is :

$$0.006 \text{ with the direct procedure}$$

$$0.003 \text{ with the indirect procedure}$$

- **Inter-hemisphere correlations :**

The assumption of independent hemispheres is the most crucial. On simulation, a correlation effect seems to exist for the direct procedure. First, the fitted value is found lower than expected as mentioned above, which reflects a drop in the r^{ideal} ratios. From the distributions of these ratios on Fig.8.b, we have estimated for this contribution an upper limit of

$$0.009$$

In the direct procedure, the accuracy on the asymptote is dominated by the double b-tag fraction $D_{bb}(\delta)$ in the denominator. It can be seen on Fig.2.b, that this fraction

happens to be very small for large values of δ , for our simulation based on a 1.2 ps b-lifetime ($D_{bb} < 0.00073$ for $\delta > 12$). With a few events left, D_{bb} become sensitive to even small residual contaminations. For data, the region near the asymptote is much more populated. There is less sensitivity, and the upper limit of 0.009 is probably pessimistic.

In the indirect procedure, the variation of the difference $(C_b(\delta) - C_b^{true}(\delta))/C_b^{true}(\delta)$ (Fig.10.a) suggests the absence of correlation on Monte-Carlo, up to $\delta = 12$. The deviation on $C_b(\delta)$ is below 1%. This gives a upper limit of 1% on relative error for the values of s_1, s_2 and 2% for the values of t_1, t_2 . Then we estimate this contribution to the error on x_b to :

$$0.004$$

- **Error due to the tagging algorithm and the modelisation :**

Misrepresentations of physical parameters, such as lifetimes or fragmentation functions, or of the precision of the vertex detector, would affect the performances of the tagging. We did not modify each of these factors to evaluate their incidence on the fitted value of x_b ; we just increased or decreased artificially the selectivity of the tagging on simulated events ⁵. The b-tag purity varied from 0.44 and 0.54 and the b-tag efficiency from 0.63 to 0.77. For this rather wide range, the convergence is more or less fast, but the value of the asymptote is almost independent of the tagging. In the Fig.10 , we have plotted the distribution of r_1 for this set of taggings around the nominal one.

This sets an upper limit for this contribution to

$$0.004$$

On real data, we have tried also a simpler tagging based on only 8 of the 12 variables previously mentioned . While the range of δ and the steepness of the drop are different, the asymptotical limit remains the same within errors.

- No difference has been found if the hemisphere axis is aligned along the x-direction (major axis of the beam spot ellipse) or y-direction.

7 Conclusions

With the direct procedure and from the ratios r_1 and r_2 , we find for the measurement of the x_b fraction inside the acceptance defined by the cosine sphericity cut at 0.75

$$\mathbf{x_b} = \mathbf{0.214} \pm \mathbf{0.010} \pm \mathbf{0.012}$$

where the main source of systematic error, which takes into account residual inter-hemisphere correlations, may be overestimated on data.

⁵We have added or subtracted one or two units of class likelihoods, if the class corresponds to the event flavour ; this was done either for a single flavour or for all flavours

Fig 10 : Influence of tagging

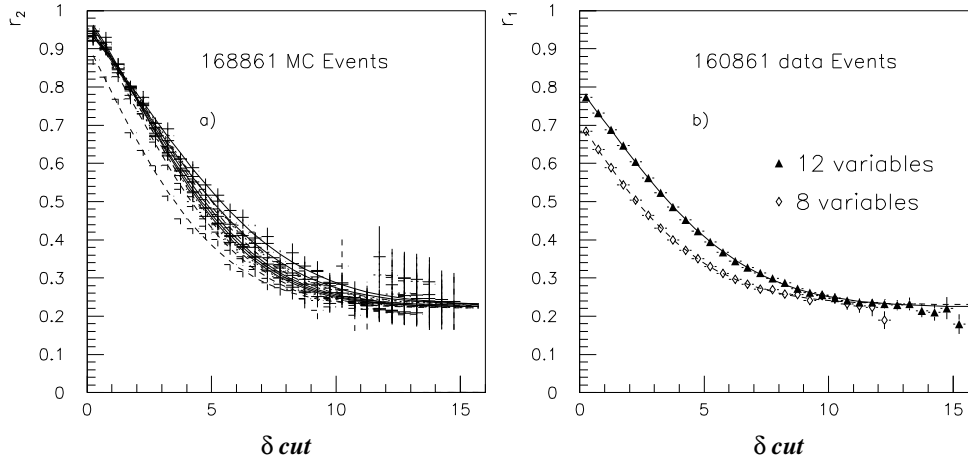


Figure 10: a) Comparison of the $r_2(\delta)$ distribution, from simulated data, for a set of modified taggings around the nominal one. b) Fits of r_1 for two taggings based on 8 and 12 variables, applied to real data.

The most accurate measurement, comes for the indirect procedure, which uses a evaluation of the probabilities $C_b(\delta)$ extracted from the data themselves. Taking the weighted average of the fits of s_2 and t_2 after smoothing of $C_b(\delta)$, we find :

$$\mathbf{x}_b = 0.220 \pm 0.004 \pm 0.006$$

fully compatible with the above result.

The indirect procedure seems to be less sensitive to possible residual inter-hemisphere correlations.

We hope to improve these results with the 1992 data (not yet fully processed through our analysis chain) : the statistics will be higher by a factor 3, and moreover the tagging selectivity could be improved by the smaller size of the beam spot and the use of RICH to identify kaons.

References

- [1] J.Bernabeu, A.Pich, A.Santamaria, CERN-TH.5931/90.
- [2] DELPHI coll. 'Classification of the hadronic decays of the Z^0 into b and c quark pairs using a neural network.' Phys. Lett. 295B(1992) 383. Bartolotto et al. 'Tagging the decays of the Z^0 boson into quark pairs with a neural network classifier' Nuclear Instrument and Methods A306(1991) 459-466 " Using Neural Networks with Jet Shapes to Identify b Jets in $e + e^-$ Interactions ". L. Bellantoni et al. CERN-PPE/91-80. 24 MAY 1991.
- [3] 'Multivariate analysis methods to tag b quark events at LEP/SLC' Brandl et Al (voir NIM)
- [4] ' B-Tagging with the DELPHI vertex detector. A direct evaluation of the $b\bar{b}$ branching ratio of the Z^0 ' E. Cortina et al. DELPHI 92-27 PHYS 163. 1992.

- [5] ' The Delphi Detector ' Delphi coll., P.AArnio et al., NIM A 303 (1991) 233-276.
- [6] Delphi coll., P.Abreu et al., Preprint CERN-PPE/92-79, to be published in Z. Phys. C..
- [7] ' B-tagging by hemisphere: description of variables and results on Monte Carlo'. P. Billoir et al. DELPHI 93-nn. 1993.
- [8] 'Direct measurement by hemisphere double tagging of the composition of hadronic samples at the Z^0 '. P. Billoir et al. DELPHI 93-nn. 1993.
Contribution to this Conference
- [9] ' A Measurement of the Partial Width of the Z^0 Boson into b Quark Pairs ' DELPHI Collaboration. CERN-PPE/90-118. 16 August 1990/ mettre a jour.
- [10] G. Anzivino et al., A263 (1988) 215-222;
M. Burns et al., CERN-EP/88-82.
- [11] R. Arnold et al., A270 (1988) 255-318.
- [12] ' Multidimensional Analysis: A Tool for B-Tagging ?' Ch de la Vaissiere, S. Palma-Lopes. DELPHI 89-32 PHYS 38. 1989.
- [13] ' CORPUS: A Heavy Quark Physics Oriented Package Preliminary Write-Up". P. Billoir et al. DELPHI 91-67. PHYS 121 PROG 175. 1991.
- [14] ' Partial Width of the Z into $b\bar{b}$ final states and Mean b Semileptonic Branching Faction". DELPHI Collaboration. Contribution to the EPS Conference in Geneva.
- [15] ' Physics Aspects if the Delphi Vertex Detector ' M. Burns et al. CERN-EP/88-82
- [16] Blue book. technical report